

## Article

# Alkali–Silica Activity and Inhibition Measures of Concrete Aggregate in Northwest China

Jing Wen <sup>1,2</sup>, Jinmei Dong <sup>1,2,\*</sup>, Chenggong Chang <sup>1,2</sup>, Xueying Xiao <sup>1,2</sup> and Weixin Zheng <sup>1,2,\*</sup> 

<sup>1</sup> Key Laboratory of Comprehensive and Highly Efficient Utilization of Salt Lake Resources, Qinghai Institute of Salt Lakes, Chinese Academy of Sciences, Xining 810008, China; wj580420@isl.ac.cn (J.W.); ccg168@isl.ac.cn (C.C.); xiaoxy@isl.ac.cn (X.X.)

<sup>2</sup> Key Laboratory of Salt Lake Resources Chemistry of Qinghai Province, Xining 810008, China

\* Correspondence: dongda839@isl.ac.cn (J.D.); zhengweixin@isl.ac.cn (W.Z.)

**Abstract:** The alkali–silica reaction (ASR)-induced expansion of mortar bars containing four types of aggregates originating from different regions in northwest China was studied. The chemical composition, mineral composition, vitreous and amorphous substances, and expansion rates were determined using X-ray fluorescence, X-ray diffraction, polarizing microscope images, and the accelerated mortar bar test (AMBT). The inhibitory effects of fly ash and silica fume on the aggregate activity were evaluated. The binary mortar mixes were produced and tested, containing cement and fly ash or silica fume as the partial cement replacement. The microstructure and composition of the ASR products were analyzed by scanning electron microscope energy dispersive spectroscopy (SEM–EDS). The results show that all four types of aggregates exhibited an alkali activity, and that all expansion rates on the 14th day were higher than the standard of 0.1%. The lowest and highest values were 0.2% and 0.3%, respectively. The primary constituent in the chemical compositions of these aggregates was found to be silica. Polarization microscopy also confirmed that they contained alkali-active cryptolites. Fly ash and silica fume could both inhibit alkali activity expansion and the silica fume exhibited a superior inhibition effect. When the fly ash and silica fume contents were 20% and 10%, respectively, the expansion rates of the mortar bar on the 14th day were all less than 0.03%.

**Keywords:** alkali aggregate reactions; fly ash; silica fume



**Citation:** Wen, J.; Dong, J.; Chang, C.; Xiao, X.; Zheng, W. Alkali–Silica Activity and Inhibition Measures of Concrete Aggregate in Northwest China. *Crystals* **2022**, *12*, 1013. <https://doi.org/10.3390/cryst12071013>

Academic Editor: Dawei Wang

Received: 4 June 2022

Accepted: 19 July 2022

Published: 21 July 2022

**Publisher's Note:** MDPI stays neutral with regard to jurisdictional claims in published maps and institutional affiliations.



**Copyright:** © 2022 by the authors. Licensee MDPI, Basel, Switzerland. This article is an open access article distributed under the terms and conditions of the Creative Commons Attribution (CC BY) license (<https://creativecommons.org/licenses/by/4.0/>).

## 1. Introduction

The alkali–silica reaction (ASR) is a chemical reaction that occurs between hydroxyl ions in the pore solution of a hydrated cement paste and in certain reactive silica phases in the aggregates used in concrete [1–5]. The reaction products may expand by imbibing water, which causes the expansion and cracking of concrete elements; this leads to the formation of the ASR gel [6–9]. Once an ASR occurs, it is difficult to prevent it; it is even more challenging to repair and save the concrete. The damage caused, which is referred to as the “cancer” of concrete, has become the second most serious disease in concrete structures, following steel corrosion [10]. ASR damage in concrete engineering was first confirmed in the United States in 1940 [11]; it has now appeared in bridges, roads, airports, ports, and industrial and civil buildings globally. Therefore, preventing and restraining the expansion of ASRs, improving concrete durability, and extending service life have become research focus areas for scientists all over the world. After more than 70 years of research, a series of achievements have been made in ASR mineral identification [12–15], test methods [16–18], inhibition measures [19–24], and model prediction [25–27].

Although the addition of silica fume or fly ash has already been extensively investigated, there are few studies on the inhibition of the alkali silica reaction of sand and gravel aggregates in Qinghai, Western China. The northwest region, particularly Tibet, is a key area for developing a strategical layout for “The Belt and Road” [28]. The infrastructure in

the area, such as railways, highways, and airports, forms the foundation of continued development [29,30]. However, the construction of the Qinghai–Tibet railway, the high-speed railway from Lanzhou to Xinjiang, airport and highway systems in the western region, and high-quality sand and stone resources have all been halted or delayed owing to potential alkali–silica activity. According to research [10,18], the concrete foundation of the Wusi bridge building in Xining was seriously damaged by ASR in 1953. The Kunlun bridge was the first viaduct in Qinghai Province, which was completed in November 2000; this bridge was also seriously damaged by ASR. Therefore, measures must be implemented to reduce or even eliminate the hidden dangers of ASRs in infrastructure projects in the Qinghai–Tibet region.

In this study, the alkali activity of aggregates commonly used in northwest region concrete projects was analyzed by means of the accelerating mortar bar test. This experiment can provide specific experimental parameters for infrastructure projects in Qinghai. There are two innovations in this paper: (1) Based on the study of alkali activity, it is found that sand and gravel aggregates in Qinghai generally have alkali–silica reactivity, which cannot be directly used in the process of concrete mix design. Preventive measures must be taken to restrain their expansion to prevent ASR damage to concrete structures. (2) On the basis of existing research, the inhibition effect of different replacement amounts of fly ash and silica fume on the alkali silica reaction of mortar is further clarified, which provides specific experimental parameters for infrastructure projects in Qinghai.

Therefore, in this work, either fly ash or silica fume were used as partial replacements for cement, and their effectiveness on the ASR expansion was studied. Microstructural analysis using scanning electron micrographs (SEM) and energy-dispersive X-ray spectroscopy (EDS) was performed; this was aimed at obtaining insights into the ASR products and the resulting expansions observed for mortar mixtures containing different percentages of fly ash and silica fume. The purpose of this study is to provide a reference value for optimizing the mix ratio of high-performance concrete in northwest China.

## 2. Materials and Experiment

### 2.1. Materials

Type I Portland cement 52.5R with an equivalent alkali cement ( $\text{Na}_2\text{O}_{\text{eq}}$ ) of 0.88 wt% was used. The fly ash was produced by the Suyuan Company of the Zhenjiang Jianbi Power Plant, with a specific surface area of  $454 \text{ m}^2/\text{kg}$  and an apparent density of  $2.2 \text{ g}/\text{cm}^3$ . The silica fume was produced by Guizhou Haitian Iron Alloy Abrasive Co., Ltd. (Guiyang, China), and its specific surface area was  $22,205 \text{ m}^2/\text{kg}$ . The chemical compositions of the cement, fly ash, and silica fume are summarized in Table 1. The phase compositions and microscopic morphologies of the fly ash and silica fume are shown in Figures 1 and 2, respectively.

**Table 1.** Chemical compositions of the cement and admixture.

Content/wt%	CaO	SiO <sub>2</sub>	Al <sub>2</sub> O <sub>3</sub>	Fe <sub>2</sub> O <sub>3</sub>	MgO	SO <sub>3</sub>	R <sub>2</sub> O	LOI
Cement	63.82	20.43	4.83	2.79	1.53	2.05	0.88	2.89
Fly ash	4.77	54.88	26.89	6.49	1.31	1.16	1.57	3.10
Silica fume	1.72	92.00	0.78	0.79	2.71	1.16	-	4.67

After investigating the natural sand commonly used in concrete engineering in the Northwest area, four types of quartz sand were selected as the research aggregates; these were obtained from the Datong, Ledu, Xining, and Minhe counties of Qinghai Province. To meet the requirements of standardized grain size distribution [31], the four aggregate types were pre-treated by washing, drying, crushing, screening, and weighing. The abbreviations, gradations, and percentage contents of the four types of quartz sand aggregates are presented in Tables 2 and 3.

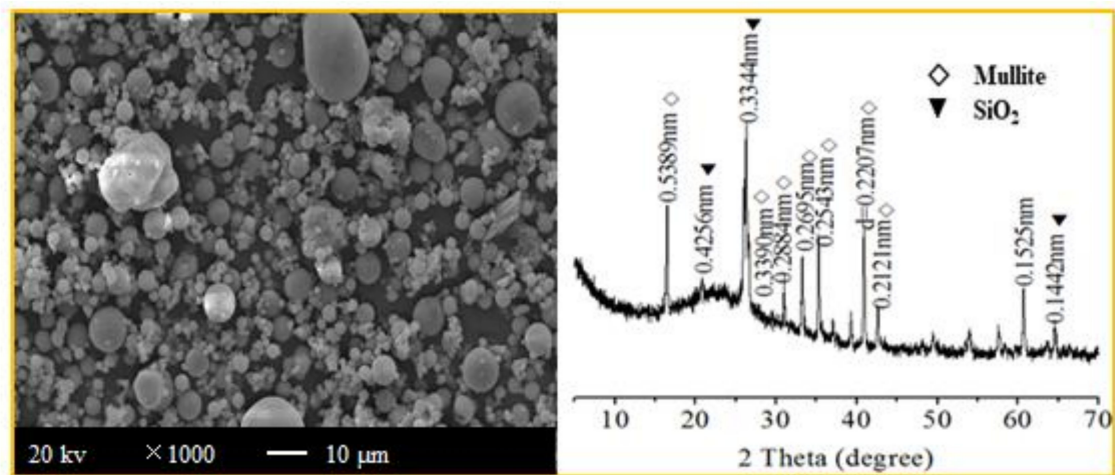


Figure 1. Phase composition and microscopic morphology of the fly ash.

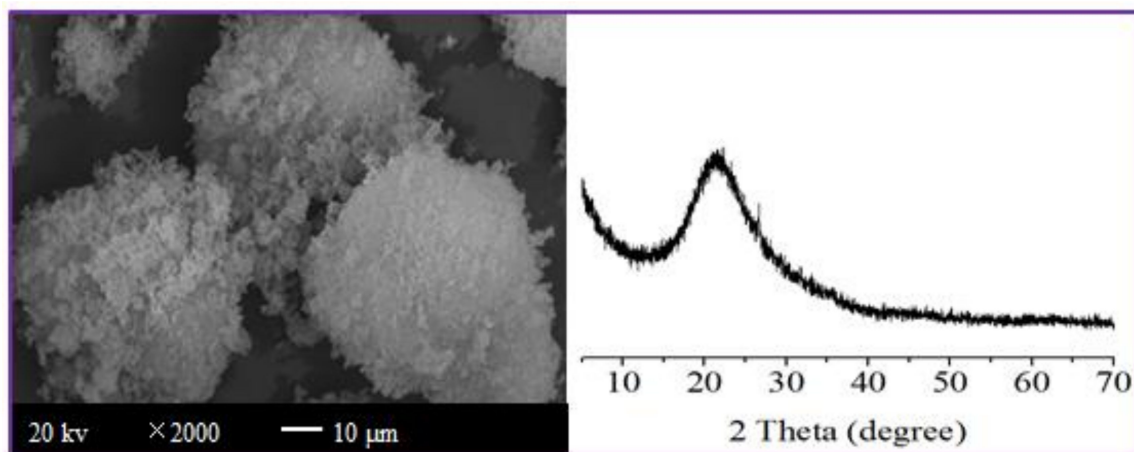


Figure 2. Phase composition and microscopic morphology of the silica fume.

Table 2. Abbreviations, gradations, and percentage contents of the four types of quartz sand aggregates.

Region	Datong	Ledu	Xining	Minhe
Abbreviation	QH1	QH2	QH3	QH4

Table 3. Gradations and percentage contents of the four types of quartz sand aggregates.

Gradations/mm	4.75~2.36	2.36~1.18	1.18~0.60	0.60~0.30	0.30~0.15
Contents/wt%	10	25	25	25	15

A pure NaOH reagent and distilled water were used in the experiment.

## 2.2. Specimen Characterization

The standard used in this experiment is GB/T 14684-2011 “sand for construction” [31]. The accelerated mortar bar test (AMBT) was selected as it is well accepted as a rapid and efficient method to determine the alkali reactivity of fine aggregates. The mortar bars were cast from mixtures with a water-to-binder ratio of 0.47 and a binder-to-fine aggregate ratio of 1:2.25 [32]. Fly ash or silica fume was used as a replacement for cement in the order of 10%, 20%, and 30% or 5%, 10%, and 15%, respectively; this was aimed at studying the effectiveness on the mitigation of the ASR.

Mortar bar specimens of 25 × 25 × 285 mm were cast. The specimens were cured at room temperature for 24 h and then submerged in water at 80 °C for one day, after

which an initial measurement of the length was taken. Then, the samples were submerged in a bath of a 1 mol/L NaOH solution. The first measurement of the change in length was conducted after three days of immersion using a digital length comparator with an accuracy of 0.001 mm. The measurements were then continued at 7, 14, and 28 days, and so on. Measurements were taken within 15 s of removing the samples from the solution.

The samples were crushed and ground in order to be tested using 200 mesh for the XRD and XRF tests. X-ray diffraction (XRD; PANalytical X'pert Pro; Cu K $\alpha$  radiation at 40 kV/30 mA and a scan rate of 0.02°/s), X-ray fluorescence (XRF; Axios PW4400, Cu K $\alpha$  radiation at 40 kV/30 mA and a scan rate: 0.02°/s), and a polarizing microscope were utilized to determine the mineralogical characteristics of the aggregates [33]. The microstructures and compositions of the ASR products were analyzed by SEM-EDS (JSM-5610LV, acceleration voltage of 20 kV) [32]. AMBT was employed to determine the alkali activity of the aggregates according to GB/T 14684-2011 [31]. Moreover, the inhibitory effects of fly ash and silica ash on the activity of the alkali aggregates were established according to GB/T 50733-2011 [34]. Three mortar specimens for each mixture were submerged in 1 mol/L NaOH solution in a sealed plastic container, and then stored in a chamber at 80 °C following the curing procedure described in the previous section. After 2 h of exposure in the NaOH solution, the initial mortar specimen length was measured using a digital length comparator. The subsequent specimen lengths were measured after a specified age. Each reported expansion value was the average of the measurements from the three specimens.

### 3. Results and Discussion

#### 3.1. Determination of Aggregate Activity

##### 3.1.1. Chemical Compositions of Four Types of Aggregates

The chemical compositions of the four types of aggregates were analyzed by XRF, and the results are presented in Figure 3. The results of the chemical analysis demonstrate that the aggregates mainly contained SiO<sub>2</sub>, CaO, Al<sub>2</sub>O<sub>3</sub>, Fe<sub>2</sub>O<sub>3</sub>, and MgO, among which the SiO<sub>2</sub> contents were all above 50%; this provides the conditions for aggregates to undergo basic silicic acid reactions. In contrast, the MgO content was not high; this blocked the necessary conditions for the alkali–carbonate reaction in the aggregate.

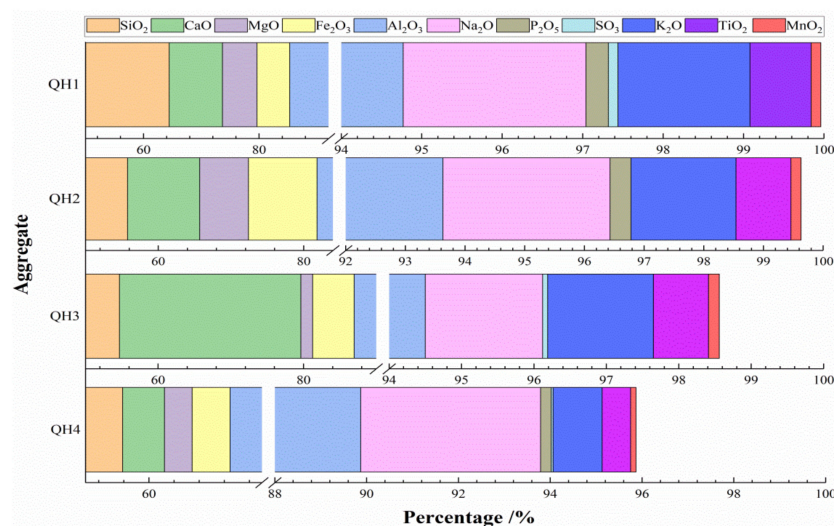


**Figure 3.** Chemical compositions of the four types of aggregates.

##### 3.1.2. Mineral Compositions of the Four Types of Aggregates

XRD analysis was performed on the aggregates to determine the main mineral compositions. The results presented in Figure 4 indicate that the main mineral compositions of the four types of aggregates were extremely complex, with each consisting of various minerals, including quartz, feldspar, and mica, as well as amorphous and vitreous substances.

The constituent minerals varied among the sources. XRD can identify crystal minerals in aggregates, but it is impossible to determine the existence of vitreous and amorphous substances in aggregates using XRD alone. The precondition for an aggregate to exhibit an alkali activity is that it contains active silica, which generally refers to amorphous silica, cryptocrystalline, microcrystalline, and vitreous silica. Therefore, petrographic analysis of the aggregates was necessary to identify their alkali activity.

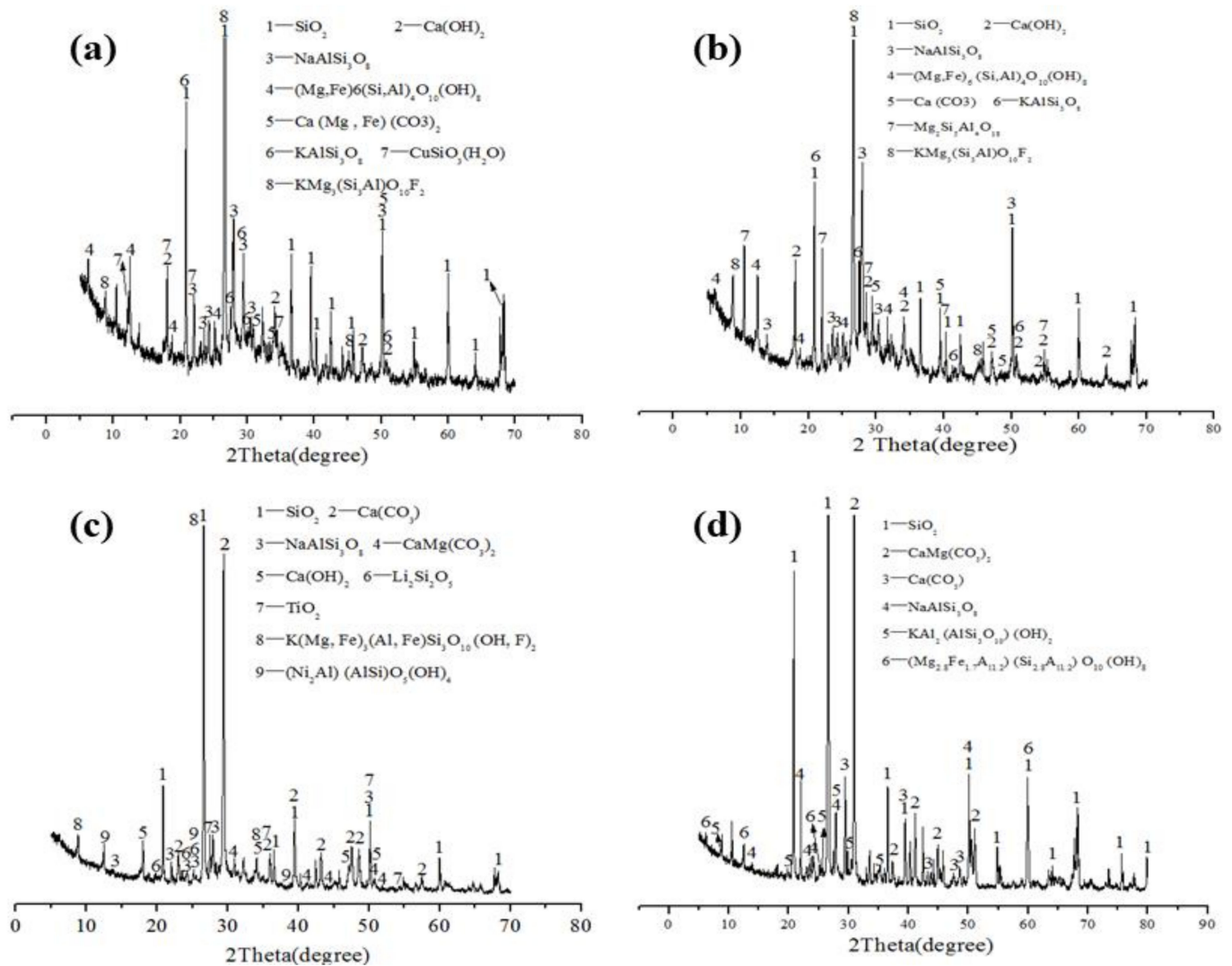


**Figure 4.** X-ray diffraction (XRD) patterns of the following four types of aggregates: (a) QH1, (b) QH2, (c) QH3, and (d) QH4.

### 3.1.3. Petrographic Analysis of Aggregates

Active silica is widely distributed in magmatic, sedimentary, and metamorphic rocks, and mainly includes amorphous-type, poor-crystallinity, and high-stress  $\text{SiO}_2$ , as well as vitreous bodies, such as opal, chalcedony, calcite, microcrystalline quartz, and quartz with a strong wave-like extinction [15,18,22]. A petrographic analysis was conducted on the four types of aggregates, and the polarizing microscope images are presented in Figure 5. The results demonstrate that there is no significant difference in the mineral compositions of the four types of aggregates, for which the main components are quartz sandstone, limestone, and mixed sandstone. The alkaline activity mainly originates from microcrystalline, cryptocrystalline, and strain quartz distributed in the limestone and miscellaneous sandstone. Furthermore, it was determined that the four types of aggregates exhibited an alkali activity and would therefore be harmful to concrete engineering. This

seems to be consistent with “alkali binding”. Shafaatian and Rajabipour [1] performs a quantitative evaluation of six potential ASR mitigation mechanisms: (1) alkali dilution, (2) alkali binding, (3) mass transport reduction, (4) increasing tensile strength, (5) altering ASR gel, and (6) reducing aggregate dissolution rate.

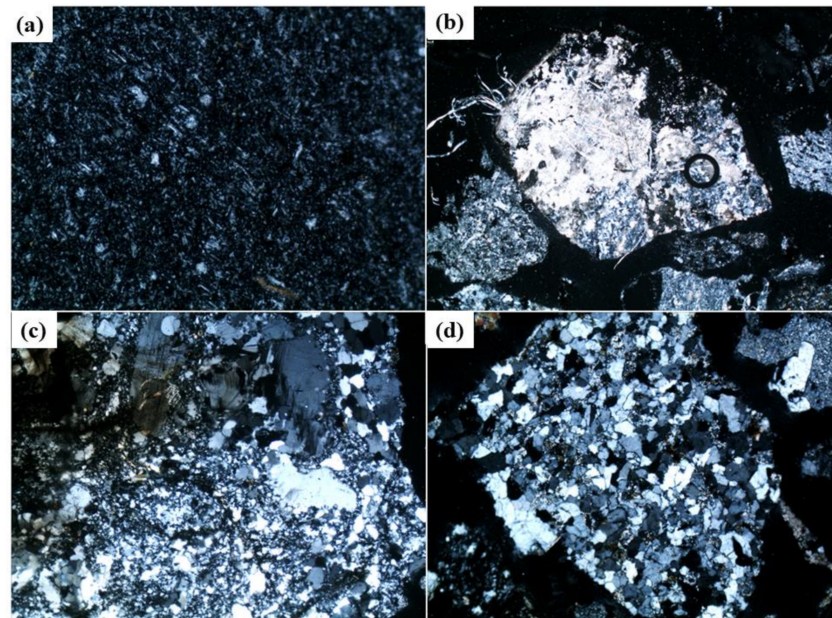


**Figure 5.** Polarizing microscope images of the four types of aggregates: (a) QH1, (b) QH2, (c) QH3, and (d) QH4.

#### 3.1.4. Expansion Rate of Four Types of Aggregates

According to the GB/T 14684-2011 standard [32], when the expansion rate of samples is less than 0.1% at 14 d, the aggregate is inactive; when the expansion rate is between 0.1% and 0.2%, it exhibits a potential alkaline activity; and when the expansion rate is greater than 0.2%, a high activity is indicated. The expansion rates of the four specimen groups at different ages are presented in Figure 6. The expansion rate of the four sample groups at 14 d is higher than the standard 0.1%, and the lowest value of the 14 d expansion rate exceeds 0.2%, while the highest value reaches 0.3%. The 28 d expansion rate increases rapidly up to between 0.3% and 0.4%. To observe the expansion failure of the aggregate during its long life, the curing period was further extended to 160 d, and the range of its expansion rate was increased to between 0.6% and 0.8%. Net-like and dendritic cracks occur on the surface of the specimen mortar bar after curing for 160 d; a white gelatinous material is found in the middle of the crack and is a symptom of alkali aggregate reaction damage. According to the chemical and mineral aggregate composition, and to the petrographic analyses, alkaline activity is common in aggregates from northwest regions; therefore, measures must be taken in the design of concrete mix proportions to prevent damage to the alkali aggregate in concrete structures.

#### 3.2. Inhibitory Effect of Fly Ash on Aggregate Alkali Activity

The aggregate QH3 was selected as the research object to explore the inhibitory effect when using an equal amount of fly ash to replace the cement, as illustrated in Figure 7. The expansion rate of the specimen gradually increases with the curing age. The addition of fly ash effectively inhibits the expansion of the alkali aggregate, with a higher fly ash content resulting in a superior inhibition effect. When the fly ash contents are 10%, 20%, and 30%, the 14 d expansion rates decrease by 57.1%, 78.6%, and 85.7%, respectively, compared with the control samples. According to the standard [34], when the 14 d expansion rate is less

than 0.03%, the admixture can effectively inhibit the expansion of ASR; therefore, a fly ash content of 20% or more can effectively inhibit the expansion of ASR in the aggregate.

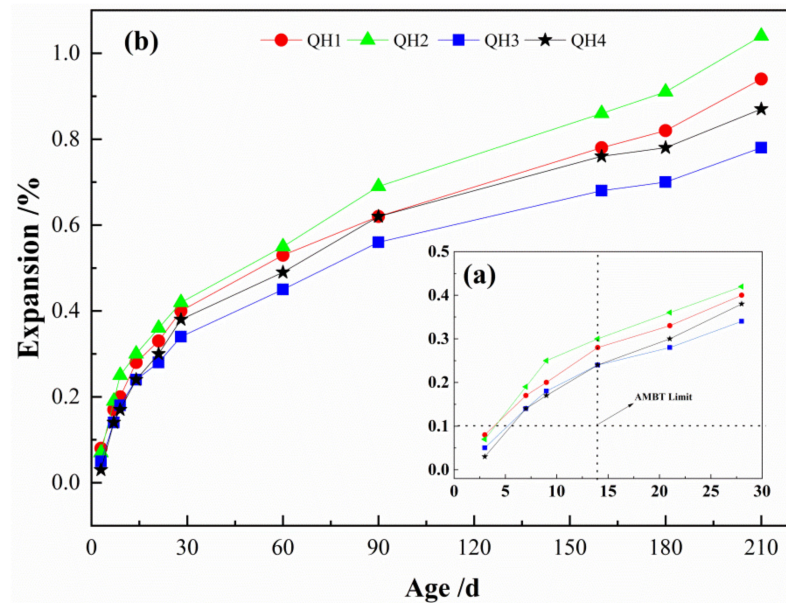


Figure 6. Expansion rate of sands in accelerated mortar bar tests (AMBT): (a) short-term and (b) long term.

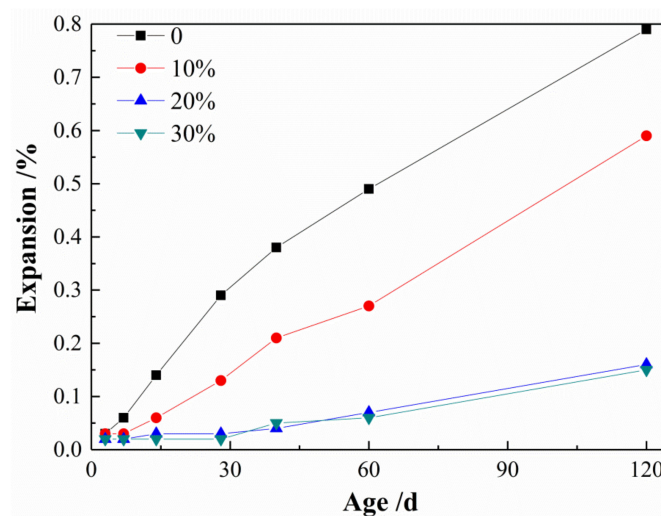


Figure 7. Effect of fly ash content on the mortar rod expansion rate.

When further extending the curing age to 60 d, the expansion rates of the blank specimens rapidly reach 0.49%, with the values being 42.6%, 85.1%, and 87.2% higher than those of the specimens mixed with 10%, 20%, and 30% fly ash contents, respectively. Thus, it can be concluded that fly ash has a strong effect on inhibiting the aggregate alkali activity at a curing age of 60 d.

### 3.3. Inhibitory Effect of Silica Fume on Aggregate Alkali Activity

Figure 8 illustrates the effect of silica fume on the inhibition of the active aggregate QH3. The addition of silica fume can effectively inhibit the expansion of the alkali aggregate, and a higher silica fume content results in a superior inhibition effect. When the silica fume contents are 5%, 10%, and 15%, the 14 d expansion rates decrease by 64.3%, 78.6%, and 78.6%, respectively, compared with the control samples. According to the standard [34], a silica fume content of 10% or more can effectively inhibit the expansion of ASR in the aggregate. Similar to the fly ash inhibition experiment, the curing age was further extended

to 60 d; then, the expansion rates of the blank specimens are 27.7%, 55.3%, and 74.5% higher than the specimens mixed with 5%, 10%, and 15% silica fume contents, respectively. It can be concluded that silica fume has a strong effect on inhibiting the aggregate alkali activity at a curing age of 60 d.

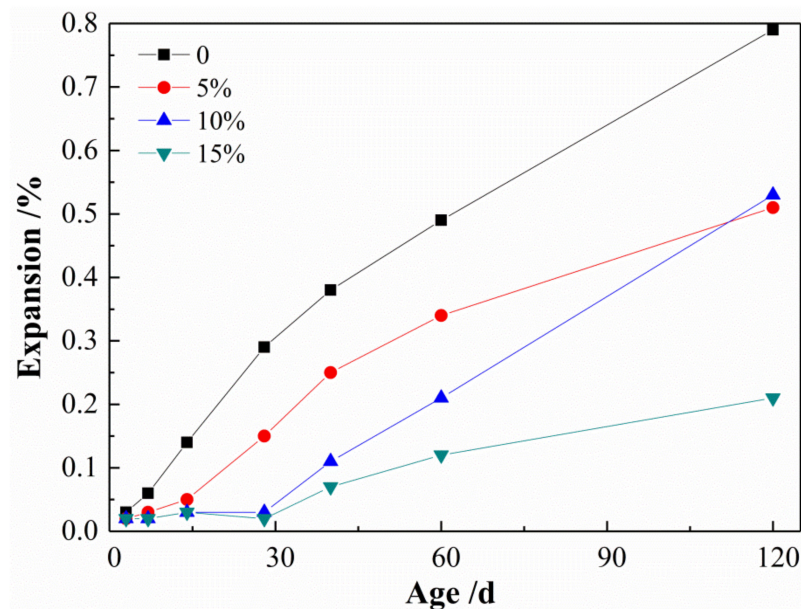


Figure 8. Effect of silica fume content on the mortar rod expansion rate.

### 3.4. Comparison of Inhibition Effect between Fly Ash and Silica Fume

A comparison of the inhibiting effects of fly ash and silica fume on the aggregate alkali activity (Figure 9) reveals that the effects differ under the same dosage of 10%, with fly ash and silica fume both having an inhibitory effect on the expansion of the aggregate alkali activity. The expansion rate of the test piece mixed with silica fume is lower than that of the fly ash with the same amount (10%), indicating that silica fume exhibits a superior inhibitory effect over the fly ash. This conclusion is consistent with the results of Thomas [23], who also demonstrated that the inhibition effect of silica fume is superior to that of low-calcium fly ash. For example, at ages of 14, 28, 40, and 60 days, the expansion rates of silica fume specimens were 0.03%, 0.02%, 0.07%, and 0.12%, respectively, which is 50%, 84.6%, 66.7%, and 55.6% lower than those of the fly ash specimens, respectively. It is worth mentioning that the inhibition effect of fly ash is related to its variety, fineness, and chemical composition [26].

The reason for these differences relates to the chemical compositions and specific surface areas of the fly ash and silica fume. From Table 1, it can be seen that fly ash mainly consists of  $\text{SiO}_2$ ,  $\text{Al}_2\text{O}_3$ , and  $\text{CaO}$ . The mass of Si/Al/Ca is 12/6/1, and the comparative area is  $454 \text{ m}^2/\text{kg}$ . The content of  $\text{SiO}_2$  in the silica fume accounts for 90%, while the contents of  $\text{Al}_2\text{O}_3$  and  $\text{CaO}$  are very small; furthermore, the specific surface area of silica fume is 49x larger ( $22,205 \text{ m}^2/\text{kg}$ ) than that of the fly ash. Scanning electron microscopy (SEM) images show that fly ash particles are spherical and smooth (Figure 1), while silica fume particles have porous surfaces (Figure 2), resulting in a stronger alkali adsorption capacity and a better inhibition effect compared with the fly ash.

### 3.5. Analysis of Inhibition Mechanisms

The microstructures of the studied mortars after 60 d of alkaline exposure were analyzed by means of SEM-EDS. When comparing the three specimen types (Figures 10–12), a crack can be seen in the control specimen, while the ASR gel in the crack and the interface of the cement and aggregate are clearly visible. The product is mainly composed of Ca, Si, Na, Al, and Mg, and the Ca-to-Si ratio reaches up to 2.98, indicating a severe ASR [19].

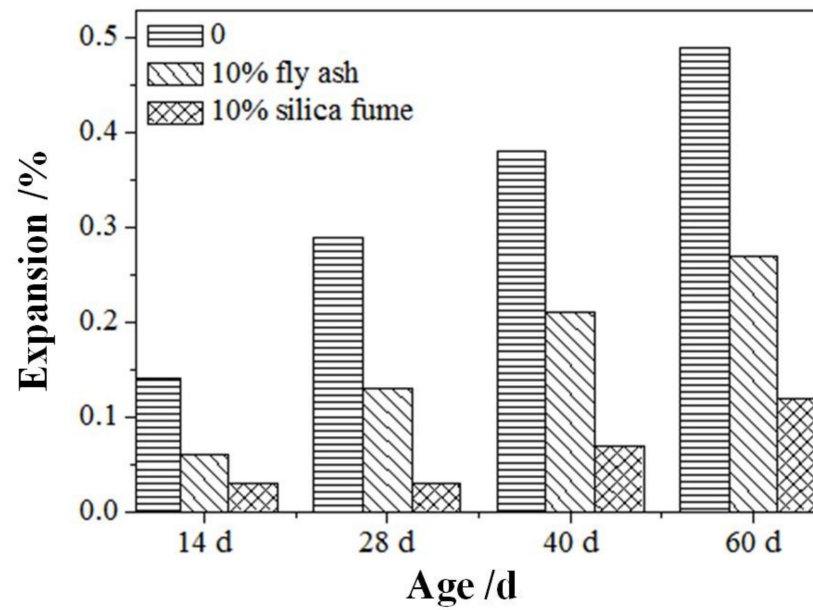


Figure 9. Expansion inhibition effects of the mortar bar for the fly ash and silica fume of 10%.

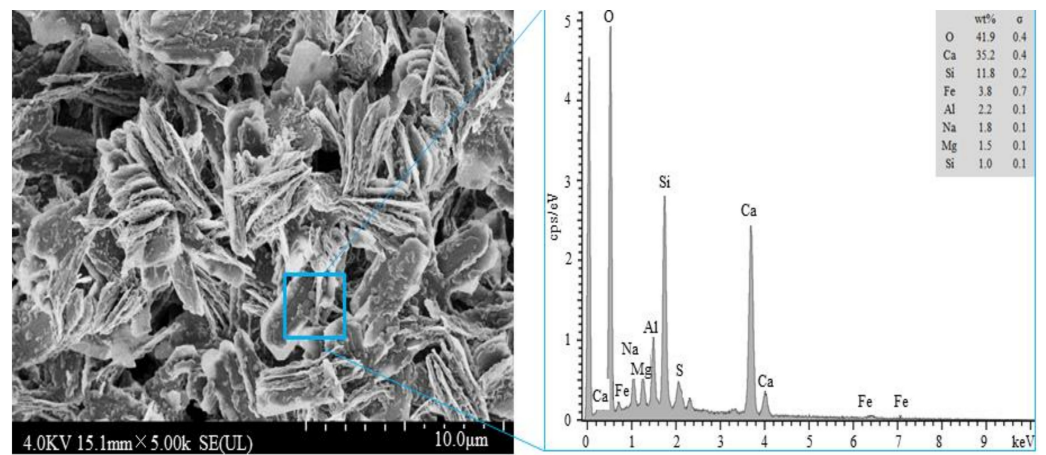


Figure 10. Scanning electron microscope energy dispersive spectroscopy (SEM-EDS) of the control sample at 60 d.

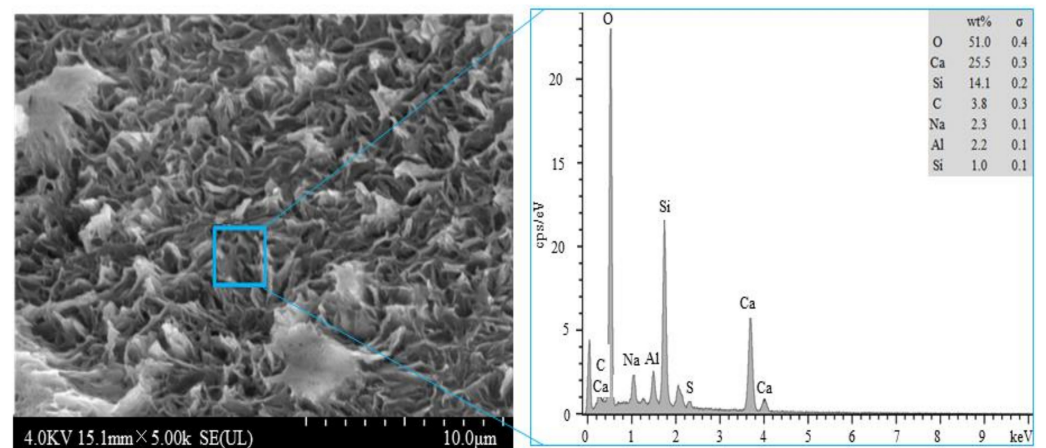
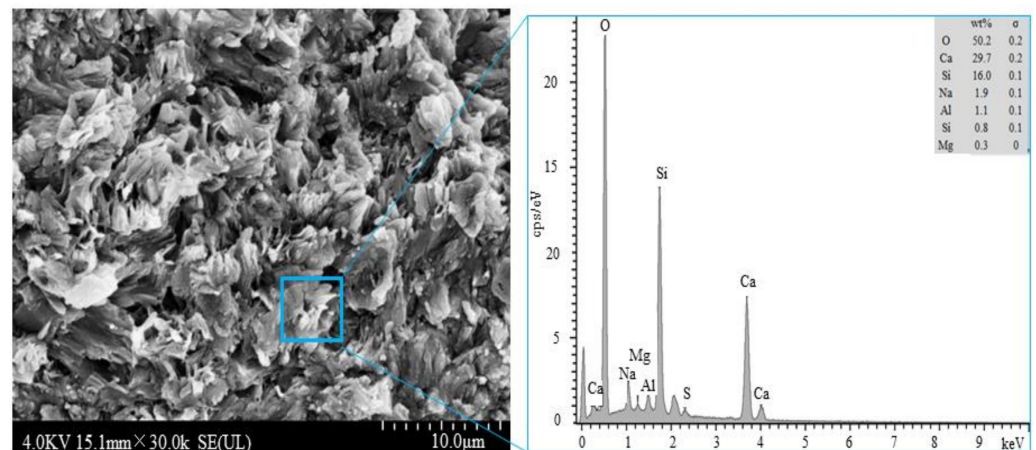


Figure 11. Scanning electron microscope energy dispersive spectroscopy (SEM-EDS) of the fly ash at 60 d.



**Figure 12.** Scanning electron microscope energy dispersive spectroscopy (SEM-EDS) of the silica sample at 60 d.

Compared with the control sample, the interface between the aggregate and cement is clear with the addition of 20% fly ash and 10% silica ash when the sample is enlarged 300 times. No reaction ring is observed and the aggregate remains intact without obvious cracks. Further amplification of the surrounding area of the aggregate reveals that the aggregate morphology is quite different from that of the control sample. The results of the energy spectrum indicate that the Ca-to-Si ratios of the fly ash and silica ash samples are only 1.81 and 1.86, respectively, which are 39.3% and 37.6% lower, respectively, than those of the control samples. The results are generally in agreement with those published by Li and Yan [35], in which a large amount of C-S-H gel with a low Ca-to-Si ratio is formed by the reaction between the fly ash and  $\text{Ca}(\text{OH})_2$ , which has been proven to be stronger and exhibit a more solid alkali ability than the CSH gel generated by pure cement hydration. Moreover, C-S-H gel with a low Ca-to-Si ratio has been found to reduce the alkali content in a pore solution as well as the ASR ability of the aggregate [36].

#### 4. Conclusions

1. Aggregates in Northwest China are generally alkaline-active and exhibit serious, harmful ASRs. Therefore, it is necessary to implement measures to prevent alkali aggregate damage in concrete structures in the concrete mix design process.
2. Standard GB/T 50733-2011 was used to evaluate the inhibitory effects of the admixtures on the activity of the aggregate base. The results demonstrate that when fly ash and silica fume dosages are more 20% and 10%, respectively, the 14 d expansion rates of the mortar bar are less than 0.03%, thereby effectively preventing the ASR of the aggregate; this provides a reference value for optimizing the mix ratio of high-performance concrete in the northwest regions.
3. The effects of fly ash and silica ash on inhibiting the alkaline activity expansion differ. For the same amounts of fly ash and silica ash (for example, 10%), silica fume exhibits a superior inhibitory effect over the fly ash. Fly ash and silica fume adsorb alkali ions by forming hydration products with a lower ca/si ratio, so as to reduce their expansion rate.

**Author Contributions:** All of the authors discussed and agreed upon the idea and made scientific contributions: writing—review and editing, writing—original draft, J.W. and W.Z.; investigation, C.C.; conceptualization, J.D.; methodology, X.X. All authors have read and agreed to the published version of the manuscript.

**Funding:** The authors would like to acknowledge the financial support from the Innovation Platform Construction Project for Key Laboratory of Salt Lake Resources Chemistry of Qinghai Province (2022-ZJ-Y06); the Youth Innovation Promotion Association of Chinese Academy of Sciences (2019423);

the Major Science and Technology Projects of Xining City, China (2019-Z-08); and the Applied Basic Research Project of Qinghai Province, China (2021-ZJ-750).

**Institutional Review Board Statement:** Not applicable.

**Informed Consent Statement:** Not applicable.

**Data Availability Statement:** Not applicable.

**Conflicts of Interest:** The authors declare no conflict of interest.

## References

1. Shafaatian, S.M.H.; Akhavan, A.; Maraghechi, H.; Rajabipour, F. How does fly ash mitigate alkali–silica reaction (ASR) in accelerated mortar bar test (ASTM C1567)? *Cem. Concr. Compos.* **2013**, *37*, 143–153. [[CrossRef](#)]
2. Saccani, A.; Manzi, S. The Role of Microstructure in Alkali–Silica Reaction Tests. *Crystals* **2022**, *12*, 646. [[CrossRef](#)]
3. Yi, L.; Mao, Z.; Deng, M.; Liu, X.; Fan, Z.; Huang, X.; Zhang, T.; Tang, M. Rapid Test Method for Evaluating Inhibiting Effectiveness of Supplementary Cementitious Materials on Alkali–Silica Reaction Expansion of Concrete. *Materials* **2022**, *15*, 3202. [[CrossRef](#)] [[PubMed](#)]
4. Juenger, M.C.G.; Ostertag, C.P. Alkali–silica reactivity of large silica fume-derived particles. *Cem. Concr. Res.* **2004**, *34*, 1389–1402. [[CrossRef](#)]
5. Maas, A.J.; Ideker, J.H.; Juenger, M.C.G. Alkali silica reactivity of agglomerated silica fume. *Cem. Concr. Res.* **2007**, *37*, 166–174. [[CrossRef](#)]
6. Glasser, L.S.; Kataoka, N. The Chemistry of ‘Alkali-Aggregate’ Reaction. *Cem. Concr. Res.* **1981**, *11*, 1–9. [[CrossRef](#)]
7. Mo, X.Y.; Yua, C.J.; Xu, Z.Z. Long-term Effectiveness and Mechanism of LiOH in Inhibiting Alkali–Silica Reaction. *Cem. Concr. Res.* **2003**, *33*, 115–119. [[CrossRef](#)]
8. Jing, L.; Masoud, M.; Yubao, Z.; Pengqiang, Z.; Maria, R.; Peyman, M. Utilizing Artificial Intelligence to Predict the Superplasticizer Demand of Self-Consolidating Concrete Incorporating Pumice, silica fume, and Fly Ash Powders. *Materials* **2021**, *14*, 6792.
9. Liu, X.; Mao, Z.; Yi, L.; Fan, Z.; Zhang, T.; Huang, X.; Deng, M.; Tang, M. Experimental Method for Evaluating the Reactivity of Alkali–Carbonate Reaction Activity. *Materials* **2022**, *15*, 2853. [[CrossRef](#)]
10. Tang, M. Classification of Alkali-aggregate Reaction. In Proceedings of the 9th International Conference on Alkali-Aggregate Reaction in Concrete, London, UK, 27–31 July 1992; Concrete Society: Camberley, UK, 1992; pp. 648–653.
11. Stanton, T.E. Expansion of Concrete Through Reaction Between Cement and Aggregate. *Proc. ASCE* **1940**, *66*, 1781–1811. [[CrossRef](#)]
12. Chen, B.; Deng, M.; Huang, X.; Mo, L.; Huang, B.; Lan, X. Siliceous and Dolomitic-bearing Aggregates Reaction in Tetramethyl Ammonium Hydroxide. *Constr. Build. Mater.* **2021**, *299*, 123948. [[CrossRef](#)]
13. Lima, S.; Gomes, T.; Moraes, J. Novel One-part Alkali-Activated Binder Produced with Coffee Husk Ash. *Mater. Lett.* **2022**, *313*, 131733. [[CrossRef](#)]
14. Yurt, Ü.; Bekar, F. Comparative Study of Hazelnut-Shell Biomass Ash and Metakaolin to Improve the Performance of Alkali-Activated Concrete: A Sustainable Greener Alternative. *Constr. Build. Mater.* **2022**, *320*, 126230. [[CrossRef](#)]
15. Wang, C.; He, H.; Wang, Y.; Xue, W. Effects of Fluorogypsum and Flue-gas Desulfurization Gypsum on the Hydration and Hardened Properties of AlkaliSlag Cement. *Crystals* **2021**, *11*, 1475. [[CrossRef](#)]
16. Lo, K.Y.; Hefny, A.M. Measurements of Residual Expansion Rates Resulting from Alkali-Aggregate Reaction in Existing Concrete Dams. *ACI Mater. J.* **1999**, *96*, 339–345.
17. Pantazopoulou, S.J.; Thomas, M.D.A. Modeling Stress-Strain Behavior of Concrete Damaged by Alkali-Aggregate Reaction (AAR). *ACI Struct. J.* **1999**, *96*, 790–798.
18. Tang, M.; Deng, M. Recent Progress of Studies on Alkali Aggregate Reaction. *J. Build. Mater.* **2003**, *6*, 1–8.
19. Lu, D.; Lu, Y.; Xu, Z.; Tang, M. Effectiveness of Fly Ash on Suppressing ASR Expansion and its Evaluation. *J. Chin. Silic. Soc.* **2003**, *31*, 498–593.
20. Mo, X. Laboratory Study of LiOH in Inhibiting Alkali–Silica Reaction at 20 °C: A Contribution. *Cem. Concr. Res.* **2005**, *35*, 499–504. [[CrossRef](#)]
21. Mo, I.X.Y.; Xu, Z.Z.; Wu, K.R.; Tang, M.S. Effectiveness of LiOH in Inhibiting Alkali-Aggregate Reaction and its Mechanism. *Mater. Struct.* **2005**, *38*, 57–61. [[CrossRef](#)]
22. Mo, X.; Jin, T.; Li, G.; Wang, K.; Xu, Z.; Tang, M. Alkali-Aggregate Reaction Suppressed by Chemical Admixture at 80 °C. *Constr. Build. Mater.* **2005**, *19*, 473–479. [[CrossRef](#)]
23. Thomas, M.; Dunster, A.; Nixon, P.; Blackwell, B. Effect of Fly Ash on the Expansion of Concrete due to Alkali-Silica Reaction—Exposure Site Studies. *Cem. Concr. Compos.* **2011**, *33*, 359–367. [[CrossRef](#)]
24. Deng, Y.; Zhang, C.; Wei, X. Influence of Lithium Sulfate Addition on the Properties of Portland Cement Paste. *Constr. Build. Mater.* **2014**, *50*, 457–462. [[CrossRef](#)]
25. Pan, J.; Feng, Y.T.; Jin, F. Meso-Scale Particle Modeling of Concrete Deterioration Caused by Alkali-Aggregate Reaction. *Int. J. Numer. Anal. Met.* **2012**, *37*, 2690–2705. [[CrossRef](#)]

26. Saha, A.K.; Khan, M.N.N.; Sarker, P.K.; Shaikh, F.A.; Pramanik, A. The ASR Mechanism of Reactive Aggregates in Concrete and its Mitigation by Fly Ash: A Critical Review. *Constr. Build. Mater.* **2018**, *171*, 743–758. [[CrossRef](#)]
27. Lu, D.; Xu, Z.; Tang, M. ASR Models for Siliceous Aggregates with Different Texture and Structure Characteristics. *J. Chin. Silic. Soc.* **2002**, *30*, 149–154.
28. Du, J.; Zhang, X.; Huang, T.; Li, M.; Ga, Z.; Ge, H.; Wang, Z.; Gao, H.; Ma, J. Trade-Driven Black Carbon Climate Forcing and Environmental Equality Under China's West-East Energy Transmission. *J. Clean. Prod.* **2021**, *313*, 127896. [[CrossRef](#)]
29. Zheng, W.; Chang, C.; Xiao, X.; Zhou, Y.; Dong, J.; Li, Y.; Wen, J.; Huang, Q.; Man, Y.A.D. Study on Applicability of Foaming Agent to Magnesium Oxochloride Cement. *J. Salt Lake Res.* **2019**, *27*, 62–69.
30. Zheng, W.X.; Xiao, X.Y.; Chang, C.G.; Dong, J.D.; Wen, J.; Huang, Q.; Zhou, Y.; Li, Y. Characterizing Properties of Magnesium Oxochloride Cement Concrete Pavement. *J. Cent. South Univ.* **2019**, *26*, 3410–3419. [[CrossRef](#)]
31. Cheng, J.L.; Yang, B.; Zhou, W.J.; Shang, Z.K.; Yao, L.J.; Hang, R.M.; Gao, C.; Xu, L.; Zhang, Y.M.; Yang, Q.S.; et al. *GB/T14684-2011; Sand of Construction*. Standardization Administration: Beijing, China, 2012.
32. Huang, Q.; Zheng, W.; Xiao, X.; Dong, J.; Wen, J.; Chang, C. Effects of Fly Ash, Phosphoric Acid, and Nano-silica on the Properties of Magnesium Oxochloride Cement. *Ceram. Int.* **2021**, *47*, 34341–34351. [[CrossRef](#)]
33. Huang, Q.; Zheng, W.; Xiao, X.; Dong, J.; Wen, J.; Chang, C. A study on the Salt Attack Performance of Magnesium Oxochloride Cement in Different Salt Environments. *Constr. Build. Mater.* **2022**, *320*, 126224. [[CrossRef](#)]
34. Ding, W.; Len, F.G.; Lu, D.Y.; Wang, L.; Fen, H.M.; Zhou, Y.X.; Hao, T.Y.; Xie, Y.J.; Li, P.X.; Zhang, J.B.; et al. *GB/T50733-2011; Technical Code for Prevention of Alkali-Aggregate Reaction in Concrete*. Ministry of Housing and Urban-Rural Development: Beijing, China, 2012.
35. Li, X.; Yan, P.Y. Influence of Fly Ash Content on Alkalinity of Pore Solution and Microstructure of Cement Pastes. *J. Build. Mater.* **2010**, *13*, 787–791.
36. Wang, W.C. Effects of Fly Ash and Lithium Compounds on the Water-Soluble Alkali and Lithium Content of Cement Specimens. *Constr. Build. Mater.* **2014**, *50*, 727–735. [[CrossRef](#)]